Neutralization of West Nile virus by cross-linking of its surface proteins with Fab fragments of the human monoclonal antibody CR4354

Bärbel Kaufmann[a], Matthew R. Vogt[b], Jaap Goudsmit[c], Heather A. Holdaway[a], Anastasia A. Aksyuk[a], Paul R. Chipman[a], Richard J. Kuhn[a], Michael S. Diamond[b,d,e], and Michael G. Rossmann[a,1]

[a]Department of Biological Sciences, Purdue University, West Lafayette, IN 47907-2054; Departments of [b]Pathology and Immunology, [d]Molecular Microbiology, and [e]Medicine, The Washington University School of Medicine, St. Louis, MO 63110; and [c]Crucell Holland BV, 2301 CA Leiden, The Netherlands

Edited by Charles M. Rice, The Rockefeller University, New York, NY, and approved September 24, 2010 (received for review July 27, 2010)

Many flaviviruses are significant human pathogens, with the humoral immune response playing an essential role in restricting infection and disease. CR4354, a human monoclonal antibody isolated from a patient, neutralizes West Nile virus (WNV) infection at a post-attachment stage in the viral life-cycle. Here, we determined the structure of WNV complexed with Fab fragments of CR4354 using cryoelectron microscopy. The outer glycoprotein shell of a mature WNV particle is formed by 30 rafts of three homodimers of the viral surface protein E. CR4354 binds to a discontinuous epitope formed by protein segments from two neighboring E molecules, but does not cause any detectable structural disturbance on the viral surface. The epitope occurs at two independent positions within an icosahedral asymmetric unit, resulting in 120 binding sites on the viral surface. The cross-linking of the six E monomers within one raft by four CR4354 Fab fragments suggests that the antibody neutralizes WNV by blocking the pH-induced rearrangement of the E protein required for virus fusion with the endosomal membrane.

antibody | cryoelectron microscopy | flavivirus

West Nile virus (WNV) is a human pathogen that causes a febrile illness, which can progress to encephalitis, paralysis, and death. The virus is endemic in parts of Africa, Asia, and Europe, and in the past decade has spread throughout North America and into Central and South America (1). WNV is closely related to other arthropod-transmitted, medically relevant flaviviruses, such as dengue, yellow fever, Japanese encephalitis, and tick-borne encephalitis viruses. These lipid-enveloped viruses enter host cells by receptor-mediated endocytosis. The single-stranded, positive-sense RNA genome is released into the cytoplasm after low pH induces the fusion of the viral lipid envelope with the endosomal membrane.

Mature WNV virions are roughly spherical with a diameter of about 500 Å. The outer viral surface is composed of an icosahedral scaffold of 180 closely packed copies of the membrane-anchored envelope (E) glycoprotein. Sets of three, nearly parallel E homodimers are associated into rafts that form a herringbone pattern on the surface of mature virions. The ectodomain of E has three structural domains, DI, DII, and DIII (2–5), with domain DI positioned structurally between DII and DIII. DII contains a fusion loop at its distal end that is indispensable for virus-cell membrane fusion. The Ig-like C-terminal domain DIII undergoes a major, pH-triggered positional rearrangement essential for fusion, and may also be involved in receptor binding (2, 6–12). During cell entry of flaviviruses, low endosomal pH triggers a proposed E protein rearrangement cascade, including the dissociation of E dimers and the outward rotation of DII during the repositioning of E monomers into fusion-active trimers (6, 9, 13).

The humoral immune response is essential for protection against flavivirus infection and disease (14, 15). The E glycoprotein is the principal antigen that elicits neutralizing antibodies against flaviviruses (16). By binding to the viral surface protein, antibodies can interfere with receptor attachment, virus internalization, or membrane fusion. Although the most potent inhibitory mouse antibodies against WNV bind to DIII of E (17–19), these appear to play a less dominant role in the human immune response against WNV infection (20). CR4354 is a strongly neutralizing human monoclonal antibody (MAb) against WNV that was isolated from a patient infected with WNV and inhibits infection subsequent to cell attachment (21). This antibody blocks virus fusion with liposomes in vitro and recognizes virus particles, but not the recombinant E ectodomain, suggesting that its epitope requires an oligomeric E arrangement present only in virions or subviral particles (SVP). Analysis of neutralization escape mutants identified residue Lys136 close to the flexible DI-DII hinge interface as part of the CR4354 epitope and showed that this amino acid is critical for antibody binding.

Here, we report the 3D cryoelectron microscopy (cryoEM) image reconstruction of WNV in complex with Fab fragments of the neutralizing antibody CR4354. The fitting of the atomic coordinates of the E glycoprotein and CR4354 Fab into the density showed that the discontinuous CR4354 epitope is formed by protein segments from two neighboring E monomers. Lys136 was confirmed as part of the epitope. The cross-linking of neighboring E monomers within a raft by the Fab fragments suggests that CR4354 neutralizes WNV infection by locking the virion in a conformation typical for mature virions, thereby prohibiting the rearrangement of E molecules into a fusion-active state necessary for infection of the host cell.

Results

CryoEM Structure of the WNV–CR4354 Fab Complex. Previous functional studies have shown that the neutralizing human MAb CR4354 does not bind to recombinant E glycoprotein, presumably because of its dependence on an oligomeric epitope. As the structural identification of the epitope would not be possible by cocrystallization of isolated E and MAb CR4354, a cryoEM study on WNV virions complexed with CR4354 Fab fragments was performed (Fig. 1). Fab fragments were used for the formation of the complex instead of whole antibodies to prevent aggregation and to avoid introduction of asymmetry incompatible with the icosahedral symmetry averaging imposed during structure determination.

Author contributions: B.K. and M.G.R. designed research; B.K., M.R.V., H.A.H., A.A.A., and P.R.C. performed research; J.G. contributed new reagents/analytic tools; B.K. analyzed data; and B.K., R.J.K., M.S.D., and M.G.R. wrote the paper.

The authors declare no conflict of interest.

This article is a PNAS Direct Submission.

Data deposition: The atomic coordinates and structure factors have been deposited in the Protein Data Bank, www.pdb.org (PDB ID codes 3N9G and 3IYW). The cryoEM density map of the WNV–Fab complex have been deposited in the Electron Microscopy Data Bank (accession no. EMD-5190), and complete coding regions have been deposited in the GenBank database (accession nos. FB580561.1 and FB580565.1).

[1]To whom correspondence should be addressed. E-mail: mr@purdue.edu.

This article contains supporting information online at www.pnas.org/lookup/suppl/doi:10.1073/pnas.1011036107/-/DCSupplemental.

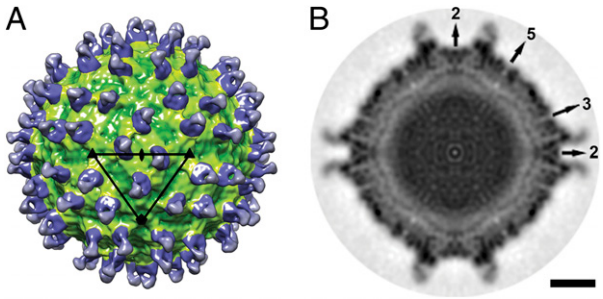

Fig. 1. CryoEM reconstruction of WNV in complex with Fab fragments of the neutralizing human MAb CR4354. (*A*) Surface rendering of the 3D image reconstruction of WNV (green) in complex with Fab CR4354 (blue) at 13.7-Å resolution, viewed down an icosahedral twofold axis. The black triangle outlines an ASU. (*B*) Central cross-section of the 3D image reconstruction of the complex viewed down an icosahedral twofold axis. The positions of icosahedral two-, three-, and fivefold axes are indicated. (Scale bar, 100 Å.)

CR4354 IgG and Fab fragments neutralize WNV infection efficiently (Fig. S1), establishing that antibody bivalency is not required for neutralization. Hence, the use of Fabs should be sufficient for evaluating the mechanism of neutralization.

The 3D cryoEM density map of the WNV–CR4354 Fab complex had an estimated resolution of 13.7 Å (Fig. 1). The glycoprotein shell and the two membrane leaflets were clearly resolved, demonstrating the quality of the map. Within the limits of the resolution, the fitting of the X-ray coordinates of the WNV E protein into the cryoEM density did not indicate any changes in the arrangement of E with respect to uncomplexed mature WNV, in which the viral surface is formed by rafts of three almost parallel E homodimers (Fig. 2). Thus, CR4354 Fab binding does not induce disturbance in the outer E protein shell, as was observed for the interaction of dengue virus with Fab fragments of 1A1D-2, a neutralizing mouse MAb that binds an epitope in DIII of the E protein (22).

CR4354 Fab binds to two independent positions (assigned labels: X1 close to threefold symmetry axis and X2 close to fivefold axis) within an icosahedral asymmetric unit (ASU), each of which is repeated 60 times on the viral surface by means of icosahedral symmetry, resulting in a total of 120 binding sites (Figs. 1 and 2). The density related to the variable domains of the Fab fragments was almost as strong as the density of the glycoprotein shell, indicating ~90% occupancy of the 120 binding sites (87% for X1, 93% for X2). The density related to the constant regions of Fab CR4354 is only about 0.7-fold as strong as the variable region, suggesting flexibility of the elbow angle between variable and constant domains, as often observed with antibody structures (23–27).

Oligomeric Epitope of MAb CR4354. To aid in the analysis of the WNV-CR4354 contact interface, CR4354 Fab was crystallized and its structure was solved to 1.4 Å resolution (Tables S1 and S2 and Fig. S2). The atomic coordinates of the E glycoprotein and of CR4354 Fab were then fitted into the cryoEM density to explore the WNV-MAb CR4354 contact on a molecular level (Fig. 2 and Table S3).

The atomic interaction (Van der Waals contacts, putative hydrogen bonds) between the fitted E molecules and the Fab at sites X1 and X2 were analyzed independently (Fig. 3, Fig. S3, Tables 1 and 2, and Table S4). The spatial arrangement of the E molecules at sites X1 and X2 is similar, but not identical. Extraction of consensus features between these two sites minimizes the uncertainties arising from possible induced changes in the Fab-antigen interface and from the experimental error due to limits of resolution. The elbow angles of the two CR4354 Fab molecules differed only slightly, being 167.5° for X1 and 163.3° for X2. However, the deviation of about 35° from the angle in the crystal structure illustrates the high elbow flexibility, consistent also with the lower cryoEM density height of the constant domains (see above). Presumably, the similar elbow angles in the Fab molecules bound to the independent binding sites in the cryoEM structure represent the lowest energy conformation, whereas the X-ray structure may have a slightly higher energy to achieve better crystal packing.

CR4354 binds to a discontinuous epitope formed by protein segments from two neighboring E molecules (Fig. 3 and Tables 1 and 2). The 18 consensus residues of the CR4354 epitope include A47, A49, A51–52, A133–138, A167–168, B310–312, B328, B368, and B370, where *A* and *B* indicate the origin of the residue in respect to the two E molecules forming the epitope for site X1 (for nomenclature, see Fig. 2). Lys136, identified previously by neutralization escape mutant analysis (21), was verified as a central part of the CR4354 epitope. Hydrophobic interactions account for much of the binding energy (Table 1 and Table S4). The contact surface at site X2 is somewhat larger than at X1, corresponding with the slightly higher occupancy for this site. The epitope is formed from residues originating from all three domains of E (Fig. 3 and Table 2). Most of the contact area is supplied by residues in DI and along the DI–II interface of one E molecule (~63% of the water-accessible area of the total epitope occluded by Fab binding; Table 1 and Fig. 3). Additional contacts are contributed by amino acids in DIII of the second E molecule. Little to no conservation of the identified epitope residues was observed among other flaviviruses (Fig. S4), consistent with the strict type-specificity of CR4354 for WNV (21).

Discussion

Specificity of CR4354 for Viral Particles. CR4354 binds to a discontinuous epitope formed by protein segments from two neighboring E molecules in an oligomeric arrangement specific to the mature virus surface (Figs. 2 and 3). This is consistent with the inability of CR4354 to bind to recombinant, soluble E ectodomain or recognize virus particles at low pH, which have undergone a conformational change (21). Although the epitope spreads over two molecules, weak binding of a single E molecule by CR4354 should be considered, at the least for the largest contact region on a single E molecule (DI and DI–II interface). Because of a difference in the DI–DII hinge angle, residues within the DI–II interface of the X-ray structure of the E ectodomain are displaced relative to the corresponding epitope on the mature virus. The combination of reduced contact area and altered geometry of the E molecule would make CR4354 interaction with the E monomer as seen in the X-ray structure (4, 5) unlikely. The E monomer conformation in immature WNV is virtually identical to recombinant, soluble E protein (28), and thus it is improbable that CR4354 can bind to completely immature virus, which has been demonstrated to be noninfectious (29). However, although CR4354 may not bind the static cryoEM image of the immature virion, it remains possible (and perhaps even likely) that it recognizes conformational subsets of immature virions that occur during particle "breathing" (22).

Previous functional studies had shown that CR4354 can recognize SVPs (21). These particles are formed by coexpression of E and premembrane (prM) transmembrane proteins. The surface of SVPs of tick-borne encephalitis virus (30) consists of 30 E dimers in a T = 1 icosahedral lattice, an arrangement that does not form the CR4354 epitope. However, the recognition of the partial epitope is spatially conceivable. Furthermore, this SVP structure is representative of only a subset of the heterogeneous SVP population. Because CR4354 binds SVPs, it is likely that there exists a SVP subpopulation with an E arrangement similar to mature virions, providing the complete CR4354 epitope.

A strict dependence of the binding of CR4354 on an oligomeric antigen arrangement present only in virus particles suggests that standard antigenic or diagnostic screens using recombinant E protein might fail to detect a significant fraction of the antibody

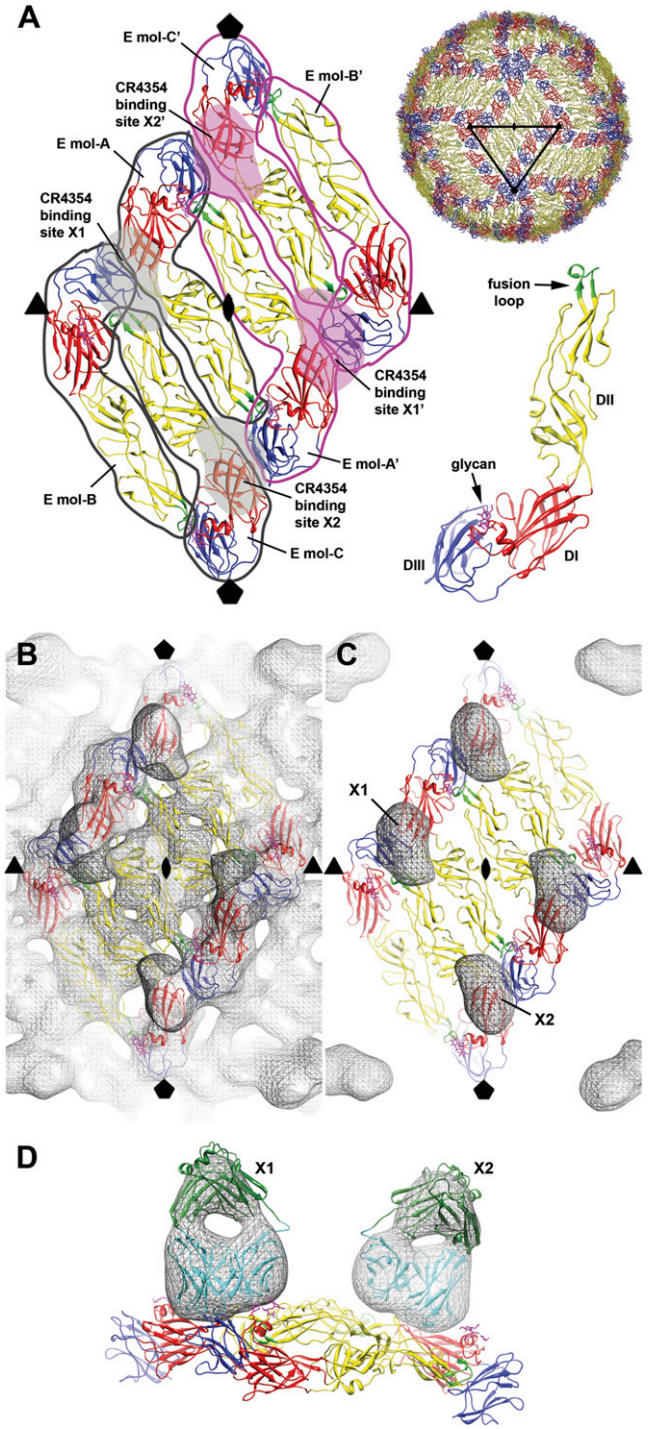

Fig. 2. Binding pattern of CR4354 relative to the E glycoprotein on the surface of mature WNV. (*A*) Arrangement of the fitted E glycoproteins on the viral surface. DI, DII, and DIII of each E monomer are colored red, yellow, and blue, respectively. The fusion loop is shown in green and N-linked glycans on DI in magenta. The gray outlines highlight the three different E monomers (E mol-A, -B, and -C) of one ASU. The typical raft structure of three almost parallel E homodimers (*Left*) is formed by the three E monomers of one ASU with the E molecules of a twofold symmetry-related ASU (E mol-A′, -B′, and -C′; magenta outlines). Gray shadows indicate the footprints of the two independent CR4354 Fab binding sites, X1 and X2, per ASU. Pink shadows show the symmetry-related Fab binding sites (X1 Vogt and X2 Vogt) in the neighboring ASU. (*B*) Fit of three independent E molecules per ASU (E mol-A through -C) into the cryoEM density of the WNV–CR4354 complex. The twofold symmetry-related E molecules (E mol-A′ through -C′) are also shown. The positions of the icosahedral five-, three-, and twofold symmetry axes are marked with symbols (pentagons, triangles, and ovals, respectively). At the chosen contour level for the complex density (2.8σ), only the variable domain density of the Fab is visible. (*C*) Difference density (gray) between the WNV–Fab complex and WNV superpositioned onto the E protein raft, viewed down an icosahedral twofold axis. The difference map is contoured as the complex density in *B*. CR4354 Fab binds to two independent sites per ASU, X1 and X2. Fab binding to X1 cross-links two E monomers of the ASU, whereas binding to X2 locks the arrangement of E in rafts by cross-linking symmetry-related E molecules. (*D*) Side view of the fitted Fab CR4354 at positions X1 and X2. The variable domains of the Fabs are shown in cyan, the constant domains in green. The difference map is contoured at 1.4σ of the complex density. Molecular graphics images were produced using Chimera (45).

repertoire. It remains to be determined if antibodies with such specificity are an important class in the protective humoral immune response against virus infections of humans or animals.

Neutralization Mechanism of CR4354. The bound CR4354 Fab fragments cross-link the six E monomers within one raft (Fig. 4), suggesting that Fab binding locks the raft organization of E in mature virions and completely blocks any pH-induced rearrangement of E before fusion with the endosomal membrane. Indeed, no structural change in the CR4354 Fab bound virion was detected when the pH environment of the complex was changed in vitro to mimic endosomal acidification, in contrast to WNV in complex with E16 Fab at low pH (31). Therefore, CR4354 most likely prohibits the dissociation of the E glycoprotein rafts before forming the fusogenic state, essentially working as a cross-linking agent of the mature virus conformation. In addition, the flexibility of the hinge angle between DI and DII, which rotates more than 30° during low pH-induced changes (32), may also be affected by CR4354 binding, thereby inhibiting the intramolecular movements required for the transition to a fusogenic trimeric E arrangement. Here, we have presented an example of a virus-antibody complex, where cryoEM structure determination has been essential in determining the complete epitope and suggesting the mechanism by which viral fusion is inhibited.

Materials and Methods

Sequencing of CR4354 Fab and Generation of a 3D Homology Model. CR4354 was selected from a single-chain variable fragment (scFv) phage display library constructed from peripheral blood lymphocytes isolated from human patients who survived neuroinvasive WNV disease (33). The reformatting of CR4354 scFv phage into full-length IgG1 was done as described previously (34). Briefly, variable heavy (V_H) and light (V_L) genes were PCR amplified using primers to restore the human framework and add restriction sites. The resulting fragments were cloned into expression vectors containing constant antibody domains ($C_{\gamma 1}$ and C_λ). The complete coding regions were deposited at the GenBank database under accession nos. FB580561.1 ($V_H + C_{\gamma 1}$) and FB580565.1 ($V_L + C_\lambda$), respectively.

A 3D homology model of the CR4354 variable domain ($V_L + V_H$) was obtained by submitting the protein sequences of heavy and light chains (Table S2) to the Web Antibody Modeling Server (WAM; http://antibody.bath.ac.uk/). Residues corresponding to the complementarity-defining regions (CDRs) in the model PDB file are: L1 (residues 23–35), L2 (51–57), L3 (90–100), H1 (26–35), H2 (50–59), and H3 (99–112). The canonical loops L1, L2, H1, and H2 were modeled with particularly high confidence.

Fab Fragment Production and Neutralization Assay. Human MAb CR4354 (subtype IgG1) was generated and purified as described elsewhere (21). Fab fragments were purified from Fc fragments, and intact MAb by protein A and size exclusion chromatography after papain digestion of the antibody (Pierce Fab Preparation Kit; Thermo Fisher Scientific). The sample was concentrated using a Vivaspin 20 centrifugal concentrator (10-kDa molecular weight cutoff; Sartorius Stedim Biotech), and Fab fragmentation was confirmed by comparing reducing and nonreducing 4–12% NuPAGE gels stained with SimplyBlue SafeStain (Invitrogen Corp.).

The neutralization capacity of the Fab fragments was compared with that of intact MAb by a plaque reduction neutralization test (PRNT) as described previously (21). Briefly, serially diluted MAb or Fab was mixed with 100 PFU of

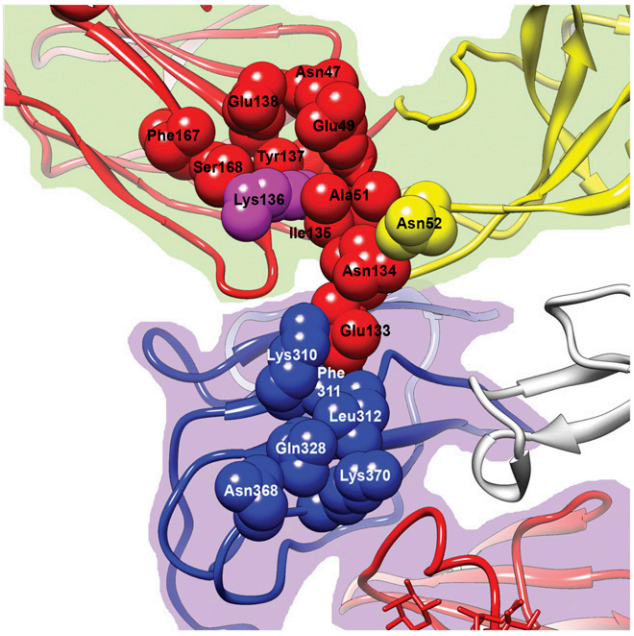

Fig. 3. Detailed view of the CR4354 epitope at binding site X1 (for binding site X2, see Fig. S3). The two independent E molecules that contribute to the CR4354 epitope are shown as ribbon diagrams and highlighted by background shading (E mol-A, green; -B, purple). The individual E domains are color-coded as follows: DI, red; DII, yellow; DIII, blue. The atoms of the E residues that constitute the CR4354 epitope are depicted as balls. Residue Lys136, previously identified as part of the epitope by neutralization escape mutant analysis (21), is shown in magenta.

WNV for 1 h at 37 °C. The mixture was added to a monolayer of BHK21-15 cells for 1 h at 37 °C, then overlaid with 1% low-melt agarose. After 3 d, the monolayer was fixed with 10% formaldehyde and stained with a crystal violet solution for visualization of plaques. Plaques were counted and then normalized to the average of six control wells in which WNV was mixed with diluent lacking MAb or Fab fragments.

Fab Fragment Crystallization and X-Ray Structure Determination. Purified Fab fragments were crystallized using the hanging-drop vapor-diffusion technique. An aliquot (1 μL) of sample in 20 mM Hepes, pH 7.4, 150 mM NaCl, 0.01% NaN_3 (protein concentration 16 mg/mL) was mixed with an equal volume of reservoir solution [20% PEG 8,000 in 10 mM Mes buffer (pH 6.0) containing 200 mM Ca

Table 1. WNV-CR4354 Fab contact analysis

Fab binding site	ASU[a]	ED[b]	OWAA[c]	VDW[d]	HB[e]
X1	A	**DI**/II	465 (465)	304 (304)	13 (13)
	B	DI/**DIII**	274 (274)	61 (61)	2 (2)
	A + B		**740 (740)**	**365 (365)**	**15 (15)**
X2[f]	C	**DI**/II	571 (440)	290 (279)	12 (11)
	A′	DI/**DIII**	404 (262)	260 (215)	10 (6)
	C + A′		**974 (702)**	**550 (494)**	**22 (17)**

For details, see Table S4. Numbers in parentheses refer to consensus residues of the independent Fab binding sites only. Values are shown for the whole epitope and each of the epitope building blocks stemming from two different E molecules.

[a]For designation of molecule position in an ASU, see Fig. 2.

[b]Domain of E to which the epitope residues map. Bold font designates major contact domain.

[c]OWAA, water-accessible area of the epitope occluded by Fab binding (in $Å^2$).

[d]VDW, number of van der Waals contacts, selected based on an interatomic distance ≤4.0 Å.

[e]HB, number of putative hydrogen bonds, predicted based on an interatomic distance ≤3.5 Å and default geometry defined in the program CONTACT.

[f]Carbohydrate contact neglected for calculations.

Table 2. The oligomeric epitope of CR4354 Fab

Epitope X1		Epitope X2		
ASU[a]	E residues[b]	ASU[a]	E residues[b]	ED[c]
A	**Asn47**, ***Glu49***, ***Ala51***, **Asn52**	C	**Asn47**, ***Glu49***, Ala50, ***Ala51***, **Asn52**	DI DII
	Glu133, ***Asn134***, Ile135, ***Lys136***, ***Tyr137***, ***Glu138***		***Glu133***, ***Asn134***, Ile135, ***Lys136***, Tyr137, ***Glu138***	DI
	Phe167, ***Ser168***		Arg166, **Phe167**, ***Ser168***, Ala172	DI
			Ser276	DII
B		A′	*Glu150*	DI
	Lys310, **Phe311**, **Leu312**		***Lys310***, **Phe311**, **Leu312**	DIII
	Gln328		***Gln328***, Thr330	DIII
	Asn368, ***Lys370***		*Thr366*, *Ala367*, ***Asn368***, Ala369, **Lys370**	DIII

WNV E residues from two neighboring E molecules that form the epitope of CR4354 Fab were selected based on an interatomic distance of 4.0 Å and are listed for both independent Fab binding sites, X1 and X2[a] (for detailed analysis, see Table S4).

[a]For designation of E molecule position in an ASU, see Fig. 2.

[b]Consensus residues, overlapping between X1 and X2, are shown in bold. Residues predicted to form hydrogen bonds with CDRs are shown in italics. Contacts between Fab and the carbohydrate moiety were ignored for epitope definition.

[c]Domain of E to which the epitope residues map.

$(OAc)_2$]. The droplet was equilibrated against 500 μL reservoir solution at 20 °C. Crystals were soaked for 1 min in the presence of 35% glycerol as a cryoprotectant before flash-freezing for X-ray data collection.

X-ray diffraction data were collected from a single frozen crystal at beamline GM/CA-CAT 23-ID-D (Advanced Photon Source, Argonne National Laboratory) using a wavelength of λ = 1.0332 Å. A total of 180 images were recorded on a Rayonix MarMosaic 300 CCD detector using a 1-s exposure time and a 1° oscillation angle per frame. The crystal to detector distance was set to 200 mm.

The diffraction data to about 1.4 Å resolution with a mosaicity of 0.16° were integrated and scaled using the HKL2000 data processing package (35) (Table S1). The orthorhombic space group $P2_12_12_1$ was assigned on the basis of symmetry and systematic absences. Assuming one Fab molecule per asymmetric unit, the Matthews coefficient V_M was 2.3 $Å^3$/Da, corresponding to a solvent content of 47%. Initial phases for the data were obtained by molecular replacement using structure factors derived from the 3D homology model of the variable domain of CR4354 Fab (V_L + V_H) and from the coordinates of the constant domain (C_L + C_{H1}) of a human IgG1 Fab (PDB accession no. 3KYK). The variable and constant domains were used as independent search models, because the hinge angle between these domains is flexible. One copy of each domain was subjected to a rotational and translational search within the asymmetric unit using Phaser of the CCP4 program suite (36). A complete Fab molecule was extracted from the molecular replacement solution.

The atomic positions were refined using the program phenix.refine of the PHENIX software suite (37, 38) (coordinate refinement: rigid body and individual, simulated annealing, gradient-driven minimization; atomic displacement parameter refinement: group, individual, TLS; occupancy refinement; automated water picking and refinement) alternated with model rebuilding into weighted 2Fo-Fc and Fo-Fc electron density maps using the interactive molecular graphics program Coot (39) (Fig. S2 and Table S1). Residue identities were corrected relative to the sequencing data, when justified by the density (Table S2). The N-terminal glutamine of chain H has cyclized to a five-membered ring structure, pyrrolidone carboxylic acid or pyroglutamic acid. An insertion of four amino acids (Ala-Ala-Ala-Gly) was detected in the elbow region of chain L, downstream of residue Gly L111. A total of 821 water molecules were tentatively placed into the density. The final R-factors for the model were 16.7% (R_{work}) and 18.6% (R_{free}). The bond lengths and angles deviated from idealized values by 0.006 Å and 1.128°, respectively. A total of 96.1% of the nonglycine, nonproline residues were within preferred regions, and 3.9% within allowed regions, of the Ramachandran plot. The elbow angle of the Fab crystal structure was determined to be 130.2° with the program RBOW (26) (http://proteinmodel.org/AS2TS/RBOW/index.html).

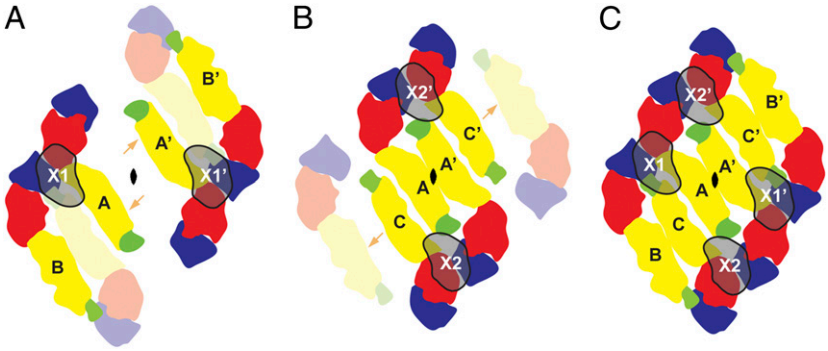

Fig. 4. The cross-linking of E molecules within a raft by CR4354 Fab fragments. Shown are the six E molecules of two twofold-related ASUs (A, B, C and A′, B′, C′) forming a raft. The position of the icosahedral twofold symmetry axis is indicated. E monomers that are engaged by a Fab are opaque. The Fab footprints at sites X1 and X2 and the twofold-related sites X1′ and X2′ are superpositioned onto the E raft. (*A*) CR4354 Fabs bound to site X1 and its twofold symmetry-related position X1′, only, engage two E molecules of one ASU each (A + B and A′ + B′, respectively). As indicated by molecule separation and arrows, this scenario possibly allows the dissociation of the central dimer upon low pH exposure. (*B*) CR4354 Fabs bound to site X2 and X2′, only, cross-link two E monomers from two neighboring ASUs each (C + A′ and C′ + A, respectively). As indicated by molecule separation and arrows, this scenario possibly allows the dissociation of the outer dimers upon low pH exposure. (*C*) Utilization of X1 and X2 results in cross-linking of all six E monomers within a raft and prohibits the dissociation of the E glycoprotein rafts before forming a fusogenic state.

Virus–Fab Complex Formation, CryoEM, and 3D Image Reconstruction. WNV was propagated and purified as described previously (31). Purified WNV particles were incubated with CR4354 Fab fragments at 37 °C for 30 min, followed by a 2-h incubation at room temperature, using a ratio of about four Fab fragments per E molecule. In parallel, the pH of an aliquot of the complex was lowered to pH 6 (low pH) using Mes-HAc buffer (0.1 M, pH 4.5) and incubated at room temperature for 5–15 min before flash-freezing. Micrographs of the frozen-hydrated sample were recorded on Kodak SO-163 films with a Philips CM300 FEG transmission electron microscope (Philips). Images were taken at a calibrated magnification of 47,244× and at a total electron dose of ~22 e^{-}/Å^2.

The cryoEM micrographs were digitized on a Nikon 9000 scanner using a 6.35-μm step size. Subsequently, sets of four pixels were averaged, resulting in a sampling of the specimen images at 2.69 Å intervals. Some 6,258 particles from 69 micrographs were boxed and processed using the program RobEM (40). The defocus levels were determined by fitting the theoretical microscope contrast transfer functions (CTF) to the incoherent average of the Fourier transforms of all particle images from each micrograph and ranged from 1.45 to 3.53 μm. A rough 3D model of the complex was generated with the Starticos program of the EMAN software package (41) by identifying particles with the best fivefold, threefold, or twofold rotational symmetry from 88 particles selected from a single CCD image. The refined 3D model calculated from the class averages for each of these three views was used to initiate the reconstruction from all available film data. The orientations and origins of all of the particles were determined by comparing the CTF-corrected particle images against reference projections of the current 3D model using the AUTO3DEM automated image reconstruction system (42). The procedure was repeated at progressively higher spatial frequencies until no further increase in the correlation coefficients was obtained. To improve the reliability of the orientation refinement, the images were band-pass filtered to reduce low- and high-frequency noise. A total of 5,006 particles were selected based on correlation between the observed image and the density projection of the current model oriented in the presumed orientation, to calculate the final 3D electron density map. The resolution of the resulting map was estimated by comparing structure factors of the virus shell computed from two independent half-data sets. The Fourier shell correlation coefficient was 0.5 at a resolution of 13.7 Å. For the final 3D reconstruction, data were included to a resolution of 13 Å, where the correlation between the two independent data sets was ~0.2.

A difference map between the WNV–Fab complex and WNV alone was calculated after scaling of the densities to optimize the radial dimensions and average density levels. The magnification of the cryoEM map was standardized to a map calculated from dengue virus model coordinates (PDB accession no. 1THD), resulting in a final pixel separation of 2.72 Å.

Fitting of Atomic Coordinates into the CryoEM Density. Initial manual placement of the E protein structure of mature WNV (27) into the WNV–CR4354 complex density suggested that the general arrangement of the E monomers in the complex was essentially the same as in mature flavivirions, indicating that Fab binding did not significantly change the conformation of the E proteins.

The atomic coordinates of E and CR4354 Fab were fitted into the cryoEM density using the program EMfit (43) (Table S3 and Fig. 2). The X-ray coordinates of the WNV E ectodomain (PDB accession no. 2HG0) were fitted into the cryoEM density of the complex constrained by icosahedral symmetry. Each of the three WNV E monomers (A, B, and C) per ASU was divided into two rigid bodies, DI + III (residues 1–51, 133–195, and 283–400) and DII (residues other than DI + III) for independent fitting. The density corresponding to the best fit of one molecule was set to zero before fitting the next molecule, to avoid steric clashes between sequentially fitted fragments. DII was fitted using a maximum distance restraint of 10 Å between the termini of strands connecting DII to DI.

The CR4354 Fab variable domain (V_L + V_H; residues L1–L115 and H1–H123) and constant domain (C_L + C_{H1}; residues L116–L220 and H124–H230) were independently fitted into the (complex-WNV) difference density map at both independent Fab positions (X1 and X2) within an ASU (Fig. 2). First, the CR4354 variable domain was fitted using main and side chain atoms (atom radius 2.7 Å). The Fab structure was completed by subsequent fitting of the Cα atoms (atom radius 6.0 Å) of the constant domain, while restraining the distance between the C and N termini of the variable and constant portion of light and heavy chains, respectively, to be less than 20 or 10 Å. The elbow angle of the resultant Fab structure was determined using the program RBOW (26).

The contact region between the E protein shell and each Fab molecule was analyzed using the programs AREAIMOL (44) and CONTACT of the CCP4 program suite (36) (Table 1 and Table S4). Van der Waals contacts (VDW) were selected based on an interatomic distance ≤4.0 Å. Putative hydrogen bonds were predicted based on an interatomic distance ≤3.5 Å and default geometry defined in the program CONTACT.

Structure Accession Numbers. The atomic coordinates and structure factors of CR4354 Fab have been deposited in the Protein Data Bank under PDB accession no. 3N9G. The cryoEM density map of the WNV–Fab complex was deposited in the Electron Microscopy Data Bank under accession no. EMD-5190. The fitted coordinates of the contents of one asymmetric unit (three E molecules and two Fab molecules) were deposited under PDB accession no. 3IYW.

ACKNOWLEDGMENTS. We are grateful to Sheryl L. Kelly for her help in the preparation of the manuscript. This work was supported by National Institutes of Health Grants R01 AI76331 (to M.G.R. and R.J.K.), R01 AI073755 (to M.S.D. and M.G.R.), and U01 AI061373 (to M.S.D.).

1. Petersen LR, Hayes EB (2008) West Nile virus in the Americas. *Med Clin North Am* 92: 1307–1322, ix.

2. Rey FA, Heinz FX, Mandl C, Kunz C, Harrison SC (1995) The envelope glycoprotein from tick-borne encephalitis virus at 2 A resolution. *Nature* 375:291–298.

3. Modis Y, Ogata S, Clements D, Harrison SC (2003) A ligand-binding pocket in the dengue virus envelope glycoprotein. *Proc Natl Acad Sci USA* 100:6986–6991.
4. Nybakken GE, Nelson CA, Chen BR, Diamond MS, Fremont DH (2006) Crystal structure of the West Nile virus envelope glycoprotein. *J Virol* 80:11467–11474.
5. Kanai R, et al. (2006) Crystal structure of West Nile virus envelope glycoprotein reveals viral surface epitopes. *J Virol* 80:11000–11008.
6. Modis Y, Ogata S, Clements D, Harrison SC (2004) Structure of the dengue virus envelope protein after membrane fusion. *Nature* 427:313–319.
7. Bhardwaj S, Holbrook M, Shope RE, Barrett AD, Watowich SJ (2001) Biophysical characterization and vector-specific antagonist activity of domain III of the tick-borne flavivirus envelope protein. *J Virol* 75:4002–4007.
8. Heinz FX, Allison SL (2003) Flavivirus structure and membrane fusion. *Adv Virus Res* 59:63–97.
9. Bressanelli S, et al. (2004) Structure of a flavivirus envelope glycoprotein in its low-pH-induced membrane fusion conformation. *EMBO J* 23:728–738.
10. Hung JJ, et al. (2004) An external loop region of domain III of dengue virus type 2 envelope protein is involved in serotype-specific binding to mosquito but not mammalian cells. *J Virol* 78:378–388.
11. Chu JJ, et al. (2005) Inhibition of West Nile virus entry by using a recombinant domain III from the envelope glycoprotein. *J Gen Virol* 86:405–412.
12. Lee JW, Chu JJ, Ng ML (2006) Quantifying the specific binding between West Nile virus envelope domain III protein and the cellular receptor alphaVbeta3 integrin. *J Biol Chem* 281:1352–1360.
13. Kuhn RJ, et al. (2002) Structure of dengue virus: Implications for flavivirus organization, maturation, and fusion. *Cell* 108:717–725.
14. Pierson TC, Fremont DH, Kuhn RJ, Diamond MS (2008) Structural insights into the mechanisms of antibody-mediated neutralization of flavivirus infection: Implications for vaccine development. *Cell Host Microbe* 4:229–238.
15. Diamond MS, Mehlhop E, Oliphant T, Samuel MA (2009) The host immunologic response to West Nile encephalitis virus. *Front Biosci* 14:3024–3034.
16. Roehrig JT (2003) Antigenic structure of flavivirus proteins. *Adv Virus Res* 59:141–175.
17. Beasley DW, Barrett AD (2002) Identification of neutralizing epitopes within structural domain III of the West Nile virus envelope protein. *J Virol* 76:13097–13100.
18. Oliphant T, et al. (2005) Development of a humanized monoclonal antibody with therapeutic potential against West Nile virus. *Nat Med* 11:522–530.
19. Sánchez MD, et al. (2005) Characterization of neutralizing antibodies to West Nile virus. *Virology* 336:70–82.
20. Oliphant T, et al. (2007) Induction of epitope-specific neutralizing antibodies against West Nile virus. *J Virol* 81:11828–11839.
21. Vogt MR, et al. (2009) Human monoclonal antibodies against West Nile virus induced by natural infection neutralize at a postattachment step. *J Virol* 83:6494–6507.
22. Lok SM, et al. (2008) Binding of a neutralizing antibody to dengue virus alters the arrangement of surface glycoproteins. *Nat Struct Mol Biol* 15:312–317.
23. Harris LJ, et al. (1992) The three-dimensional structure of an intact monoclonal antibody for canine lymphoma. *Nature* 360:369–372.
24. Guddat LW, et al. (1995) Intramolecular signaling upon complexation. *FASEB J* 9: 101–106.
25. Saphire EO, et al. (2002) Contrasting IgG structures reveal extreme asymmetry and flexibility. *J Mol Biol* 319:9–18.
26. Stanfield RL, Zemla A, Wilson IA, Rupp B (2006) Antibody elbow angles are influenced by their light chain class. *J Mol Biol* 357:1566–1574.
27. Kaufmann B, et al. (2006) West Nile virus in complex with the Fab fragment of a neutralizing monoclonal antibody. *Proc Natl Acad Sci USA* 103:12400–12404.
28. Zhang Y, Kaufmann B, Chipman PR, Kuhn RJ, Rossmann MG (2007) Structure of immature West Nile virus. *J Virol* 81:6141–6145.
29. Moesker B, Rodenhuis-Zybert IA, Meijerhof T, Wilschut J, Smit JM (2010) Characterization of the functional requirements of West Nile virus membrane fusion. *J Gen Virol* 91:389–393.
30. Ferlenghi I, et al. (2001) Molecular organization of a recombinant subviral particle from tick-borne encephalitis virus. *Mol Cell* 7:593–602.
31. Kaufmann B, et al. (2009) Capturing a flavivirus pre-fusion intermediate. *PLoS Pathog* 5:e1000672.
32. Zhang Y, et al. (2004) Conformational changes of the flavivirus E glycoprotein. *Structure* 12:1607–1618.
33. Throsby M, et al. (2006) Isolation and characterization of human monoclonal antibodies from individuals infected with West Nile Virus. *J Virol* 80:6982–6992.
34. Boel E, et al. (2000) Functional human monoclonal antibodies of all isotypes constructed from phage display library-derived single-chain Fv antibody fragments. *J Immunol Methods* 239:153–166.
35. Otwinowski Z, Minor W, Charles WC (1997) Processing of X-ray diffraction data collected in oscillation mode. *Methods in Enzymology: Macromolecular Crystallography, Part A*, eds Carter Jr, CW, Sweet RM (Academic, New York), Vol 276, pp 307–326.
36. Collaborative Computational Project, Number 4 (1994) The CCP4 suite: Programs for protein crystallography. *Acta Crystallogr D Biol Crystallogr* 50:760–763.
37. Adams PD, et al. (2002) PHENIX: Building new software for automated crystallographic structure determination. *Acta Crystallogr D Biol Crystallogr* 58:1948–1954.
38. Adams PD, et al. (2010) PHENIX: A comprehensive Python-based system for macromolecular structure solution. *Acta Crystallogr D Biol Crystallogr* 66:213–221.
39. Emsley P, Cowtan K (2004) Coot: Model-building tools for molecular graphics. *Acta Crystallogr D Biol Crystallogr* 60:2126–2132.
40. Baker TS (2004) RobEM—image processing and visualization programAvailable at http://bilbo.bio.purdue.edu/.
41. Ludtke SJ, Baldwin PR, Chiu W (1999) EMAN: Semiautomated software for high-resolution single-particle reconstructions. *J Struct Biol* 128:82–97.
42. Yan X, Sinkovits RS, Baker TS (2007) AUTO3DEM—an automated and high throughput program for image reconstruction of icosahedral particles. *J Struct Biol* 157:73–82.
43. Rossmann MG, Bernal R, Pletnev SV (2001) Combining electron microscopic with x-ray crystallographic structures. *J Struct Biol* 136:190–200.
44. Lee B, Richards FM (1971) The interpretation of protein structures: Estimation of static accessibility. *J Mol Biol* 55:379–400.
45. Pettersen EF, et al. (2004) UCSF Chimera—a visualization system for exploratory research and analysis. *J Comput Chem* 25:1605–1612.